RESEARCH ARTICLE

ADVANCED
ENERGY & SUSTAINABILITY
RESEARCH
Open Access
www.advenergysustres.com

Role of A-Site Composition in Charge Transport in Lead Iodide Perovskites

Min Ji Hong and John G. Labram*

As the power conversion efficiency and stability of solar cells based on metal halide perovskites continue to improve, the community increasingly relies on compounds formed of mixed cations and mixed halides for the highest performing devices. The result is that device engineers now have a potentially infinite number of compositions to choose from. While this has provided a large scope for optimization, it has increased complexity of the field, and the rationale for choosing one composition over another remains somewhat empirical. Herein, the distribution of electronic properties for a range of lead iodide perovskite thin films is mapped. The relative percentages of methylammonium, formamidinium, and cesium are varied, and the electronic properties are measured with time-resolved microwave conductivity, a contactless technique enabling extraction of electronic properties of isolated films of semiconductors. It is found a small amount of Cs leads to larger carrier mobilities and longer carrier lifetimes and that compositions with a tolerance factor close to 0.9 generally show lower performance that those closer to 0.8 or 1.0.

1. Introduction

Metal halide perovskites (henceforth referred to as just "perovskites" for brevity), since their first appearance as an absorber layer in solar cells in 2009,[1] have led to an explosion of academic[2] and industrial[3] interest. The power conversion efficiency (PCE) of lab-scale perovskite solar cells has surpassed that of polycrystalline silicon and is now comparable with monocrystalline silicon.[4,5] For these reasons, perovskite solar cells are hoped to play a decisive role in improving the commercial attractiveness of utility-scale solar energy production and, ultimately, in mitigating the worst effects of climate change.

M. J. Hong, J. G. Labram
School of Electrical Engineering and Computer Science
Oregon State University
Corvallis, OR 97331, USA
E-mail: j.labram@ucl.ac.uk

J. G. Labram
Department of Electronic and Electrical Engineering
University College London
London WC1E 7JE, UK

The ORCID identification number(s) for the author(s) of this article can be found under https://doi.org/10.1002/aesr.202200120.

Perovskite is the designated name for materials isostructural to ABX_3 where A and B are cations, and X is an anion, which is commonly a halide in the perovskite solar cell community. Research into perovskites started with compounds based on a single cation such as $MAPbI_3$ or $FAPbI_3$,[1,6,7] where MA is methylammonium and FA is formamidinium. Nowadays, compounds formed from mixed X-site halides and mixed A-site cations are known to generally yield greater PCE[8,9] and stability[10,11] than single-cation, single-halide systems. While extensive efforts are devoted to find the optimal composition by tuning A-site and X-site constituents,[2,12] lead (Pb) is now believed to be essential for the defect-tolerant nature of perovskites with a bandgap close to 1.5 eV.[13] For this reason, studies into B-site composition are less common for single-junction solar cells.

Modifying the composition provides a means to tune the properties of perovskite-based devices. Changing the composition of the X-site is known to strongly effect optoelectronic properties[2] and in particular the bandgap.[14] The A-site cation contributes more to structure stability, with a mixed A-site believed to frustrate the known decomposition routes for $MAPbI_3$ and $FAPbI_3$.[15] Cs doping in an FA structure showed the reduced formation of nonperovskite phases,[16,17] and triple-cation systems have shown better PCE in solar cell devices also.[8] However, most systematic studies into perovskite composition are carried out on finished solar cell devices, with the majority of conclusions drawn on perovskite properties being based on electrical parameters, such as PCE.[18]

In this work, we investigate how the electronic properties of perovskites themselves, rather than of finished devices, depend on composition. Proxies for carrier mobility and lifetime are evaluated for perovskite thin films using time-resolved microwave conductivity (TRMC). We study single-, double-, and triple-cation lead iodide perovskites and how composition effects optoelectronic properties. In order to keep this a targeted study, we here restrict our attention to the A-site cation rather than the X-site halide. Analogous studies into the role played by X-site composition have previously been carried out.[19]

2. Evaluation of Electronic Properties Via Time-Resolved Microwave Conductivity

TRMC enables one to measure changes in the conductance of thin films of semiconductors (typically deposited on quartz or

ADVANCED
SCIENCE NEWS
www.advancedsciencenews.com

ADVANCED
ENERGY & SUSTAINABILITY
RESEARCH
Open Access
www.advenergysustres.com

glass) as a function of time, in response to irradiation by a pulsed optical source.[20,21] Examples of TRMC transient photoconductance (ΔG) measured in this study are shown in **Figure 1** for various incident laser fluence values. Figure 1a shows example data for pure MAPbI$_3$, Figure 1b for MA$_{0.5}$FA$_{0.5}$PbI$_3$, and Figure 1c for (MA$_{0.17}$FA$_{0.83}$)$_{0.95}$Cs$_{0.05}$PbI$_3$. While the exact fluence values

are different for each compound, the same behavior is observed: a rapid increase in ΔG when the laser pulse is incident, followed by a slower decay as free charges recombine.

The TRMC figure of merit is $\phi\Sigma\mu$, where ϕ is carrier generation yield and $\Sigma\mu = (\mu_e + \mu_h)$ is the sum of the average mobilities of photogenerated carriers, where μ_e is the average electron mobility and μ_h is the average hole mobility, over the illuminated sample area. With knowledge of the sample absorbance, the incident number of photons, $\phi\Sigma\mu$ can be extracted from transient ΔG TRMC data.[22] $\phi\Sigma\mu$ has the same units as carrier mobility but is often lower than $\Sigma\mu$ because the conversion of absorbed photons to electron–hole pairs is rarely 100% efficient. For example, some photons will be absorbed, but form bound excitons and recombine before being able to separate into electrons and holes.[23,24] However, the exciton binding energy for most perovskites is often below the thermal energy at room temperature, and ϕ is therefore close to unity.[25] Hence the TRMC figure of merit can often be interpreted in a similar way to the sum of carrier mobilities in perovskites.

Figure 2a shows the mean value of $\phi\Sigma\mu$ for three identically processed samples, measured as a function of incident laser fluence. $\phi\Sigma\mu$ decreases as a function of incident laser fluence at
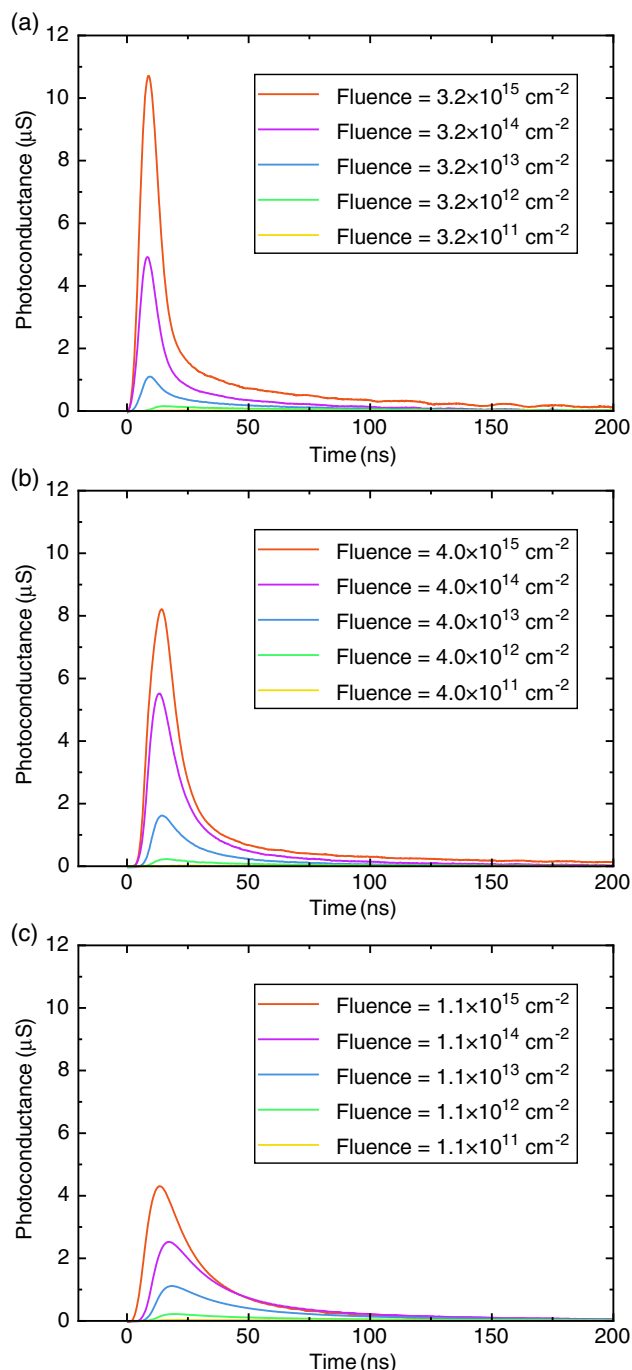

Figure 1. Photoconductance of thin films of a) MAPbI$_3$, b) MA$_{0.5}$FA$_{0.5}$PbI$_3$, and c) (MA$_{0.17}$FA$_{0.83}$)$_{0.95}$Cs$_{0.05}$PbI$_3$, as a function of time in response to irradiation with a pulsed optical laser, with various values of incident laser fluence.
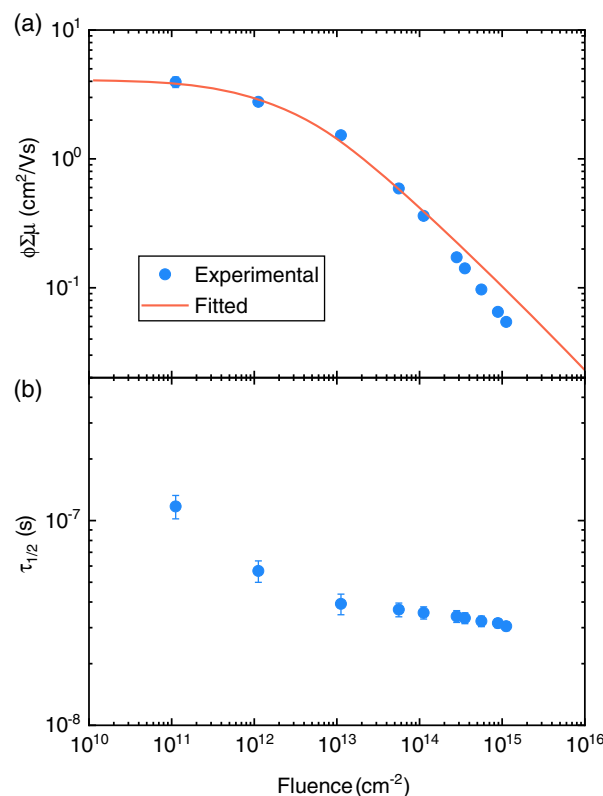

Figure 2. a) TRMC figure of merit $\phi\Sigma\mu$, as a function of fluence for thin film of (MA$_{0.17}$FA$_{0.83}$)$_{0.95}$Cs$_{0.05}$PbI$_3$. Points are average values of three different samples prepared under identical conditions and the line is a numerical model fit to the data that accounts for bimolecular and Auger recombination during the laser pulse. b) Estimated average carrier half life for the same samples of (MA$_{0.17}$FA$_{0.83}$)$_{0.95}$Cs$_{0.05}$PbI$_3$, measured as a function of fluence.

**ADVANCED
SCIENCE NEWS**

www.advancedsciencenews.com

**ADVANCED
ENERGY & SUSTAINABILITY
RESEARCH**
Open Access

www.advenergysustres.com

high fluence values but is less sensitive at lower values of fluence. This is because bimolecular and Auger recombination during the laser pulse reduce the peak observable carrier concentration when carrier density is high. Models have been developed to account for this and enable representative (fluence-independent) values of $\phi\Sigma\mu$ to be extracted from such data.[26] The red line in Figure 2a shows an example of such a fit. Reproducibility is another issue that not only inhibits commercialization of perovskites,[27] but also makes it challenging to make consistent and reproducible statements on perovskite properties.[28,29] In this study we prepared three samples for each composition and draw conclusions based on averages of the figure of merit, rather than individual samples.

The mobility of charge carriers in solar cells is a critical factor in performance, as faster moving charges are more likely to be extracted before recombining than slower charges.[30] Another crucial parameter which impacts extraction is the average lifetime of charges in the film, τ.[31] Lifetime often depends on carrier type and comprises contributions from monomolecular, bimolecular, and Auger processes.[32] For this reason, τ typically depends on carrier density, and defining a single value of τ for all conditions is challenging. Because TRMC transient data encapsulate electronic properties over several orders of magnitude of charge density,[26] TRMC transient data rarely follow a single exponential decay[33] and hence attribution of a single value of τ from TRMC data is not obvious. Instead, the photoconductance half life, $\tau_{1/2}$, is often used as a proxy for τ.[34] Half life is defined as the time it takes for photoconductance to fall from its maximum value, ΔG_{max}, to half of the maximum $\Delta G_{max}/2$.

Figure 2b shows $\tau_{1/2}$ as a function of incident laser fluence. As with $\phi\Sigma\mu$, $\tau_{1/2}$ decreases with increasing fluence, as bimolecular and Auger recombination processes increase the rate of recombination as carrier density increases. For the purposes of this study, we have simply used the unweighted average of $\tau_{1/2}$ over all measured values of fluence. We acknowledge that this value will be skewed by the higher number of measurements made at higher fluence, but since all samples were measured with comparable fluence values, and all exhibit a similar dependence of $\tau_{1/2}$ on fluence, we view this as a reasonable, albeit crude, way to compare relative recombination rates between samples.

3. Role of A-Site Composition on Electronic Properties

Analogous measurements to those depicted in Figure 2 were carried out on a range of perovskite thin films, with various compositions. The extracted mean figure of merit as a function of A-site % is shown in **Figure 3**a. This is a ternary plot, meaning the vertices represent compositions with 100% MA, FA, Cs, respectively, on the A-site. The lines moving away from these vertices represent lower values (e.g., a horizontal line through the triangle represents 50% Cs). The points show compositions which were studied, and the colors are linear interpolation between these points. For each composition studied, the average from three identically processed samples was used to evaluate the value plotted.
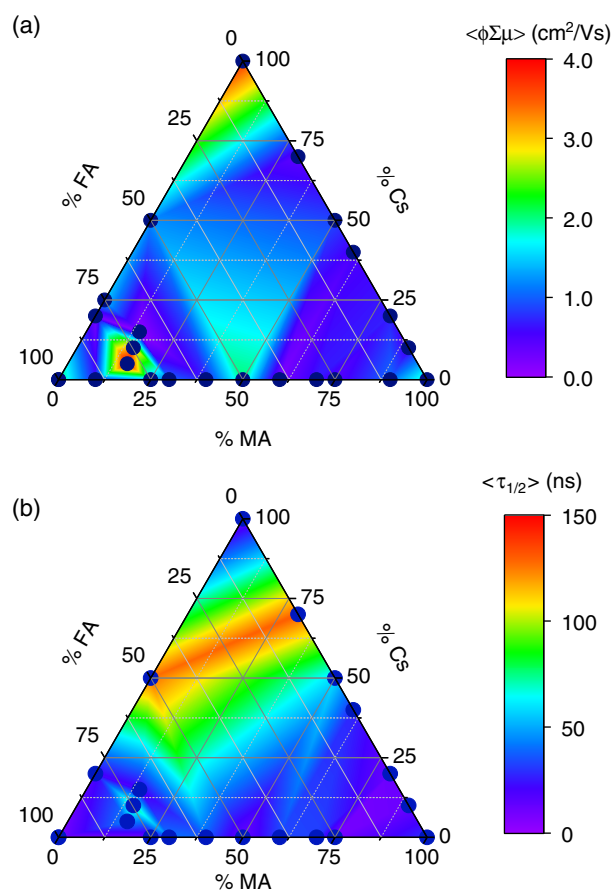

Figure 3. a) Mean TRMC figure of merit $\langle\phi\Sigma\mu\rangle$ of perovskite thin films evaluated using TRMC, as a function composition of the A-site. b) Mean carrier half life $\langle\tau_{1/2}\rangle$, of same films. Points are compositions studied and colors are interpolated between these points. For each point, the average value from three identically processed samples was used.

A wide range of factors affect mobility in perovskites, including microstructure,[35] trap states,[36] carrier density,[26] temperature, and[37] interface properties.[38] However, we do make some interesting observations when considering just the A-site composition in this way. Pure MAPbI$_3$, FAPbI$_3$, and CsPbI$_3$ exhibit relatively high mobilities. It is possible that this is due to lower in-grain energetic disorder in these systems. As mixed cation compounds will have a random cation at each A-site, not all unit cells will be the same, and we would hence expect coherence of wavefunctions to be affected over the grain. More experiments (or calculations) would of course be useful to better understand this. All measurements were carried out immediately after film fabrication and were generally concluded within 1 h. For the quasistable[8] compound CsPbI$_3$, the sample was also measured one day after measurement to determine if it had degraded. After one day, a TRMC signal was not observable for the degraded film, suggesting it was no longer optoelectronically active. We can therefore conclude that the signal measured straight after deposition (and plotted in Figure 3) is at least partially CsPbI$_3$ in a perovskite form. We however cannot say with any certainty that

**ADVANCED
SCIENCE NEWS**
www.advancedsciencenews.com

**ADVANCED
ENERGY & SUSTAINABILITY
RESEARCH**
Open Access
www.advenergysustres.com

this is pure CsPbI$_3$, but we can say there is some CsPbI$_3$ present; otherwise, we would see no signal. For this reason, we interpret this particular vertex as being the minimum $\phi\Sigma\mu$, rather than a representative value.

In most double-cation mixtures, the highest $\phi\Sigma\mu$ is obtained when each compound is mixed in the same ratio (e.g., MA$_{0.5}$FA$_{0.5}$PbI$_3$). The exception is for FACs, where the highest value was obtained when 75% of FA and 25% of Cs were mixed. While exact attribution of a certain value of $\phi\Sigma\mu$ with a certain composition is not the objective of this study, it is important to note that incorporation of small amount of cesium has been shown to yield a significant improvement in solar cell device performance.[16,39,40] In the case of triple-cation systems, as the proportion of cesium increases, mobility was observed to decrease generally. It is also important to note that the highest and the lowest average mobilities are both found in the triple-cation system.

Figure 3b shows the average half life as a function of A-site composition in the same perovskite thin films. In contrast with the mobility, lower values are found at the three vertices. Because the representative $\tau_{1/2}$ values plotted in Figure 3b are an unweighted average of $\tau_{1/2}$ extracted at all fluences, and more measurements are taken at higher fluence than low fluence (e.g., see Figure 2b), the data in Figure 3b is more representative of bimolecular processes than monomolecular process.[26] Unlike time-resolved photoluminescence (TRPL), TRMC is not sensitive to the decay of bound excitons; it is only sensitive to free charges, which often results in decay transients being observed over dissimilar timescales in the same compounds.[41] Similarly, constant bias-based techniques like transient photovoltage (TPV)[42] are also likely to probe dynamics not observed in zero-bias techniques such as TRMC or TRPL. Therefore different transient techniques can yield decay curves over very different timescales: from picoseconds[37] to milliseconds.[43] For this reason, a comparison of lifetime between techniques must be carried out with care.[32]

It is important to reiterate that the data presented in Figure 3 is the mean of three identically processed samples for every condition and that TRMC measures electronic properties over a macroscopic area (defined by laser spot size). We know that microstructure[29,35] and phase[44] have a significant impact on charge transport in this class of materials, so we would expect differences in parameters depending on processing, but we interpret the presented values as the representative average for each composition.

4. Relationship Between Properties in Lead Iodide Perovskite Thin Films

While the composition clearly does play a role in both mobility and lifetime of carriers in perovskites, it is not immediately clear why this is the case. Since microstructure is known to be affected by composition, this is a possible explanation. However, the relationship between microstructure and carrier dynamics is complex. Grain boundaries have been argued to be beneficial, neutral, and detrimental to certain aspects of perovskite solar cell performance.[45–47] For example, there is evidence from Kelvin probe force microscopy that grain boundaries help the separation of photogenerated carriers.[48] Similarly, atomic force microscopy

experiments have demonstrated that charge generation and transport are not significantly different in grains and at grain boundaries.[49] This can be rationalized by the fact that defects in perovskites can be shallow and/or inactive.[50] If grain boundaries in this class of materials were relatively benign[49] it would also be consistent with the general observation in the literature of diffusion lengths exceeding average grain sizes.[51,52] In contrast to this, there exists abundant experimental[53,54] and computational[55] evidence that charge recombination is accelerated at grain boundaries, and broadly the consensus is in community is that grain boundaries are not desirable in perovskite solar cells.[56–59]

In our case, it is unlikely that microstructure alone is responsible for the variations in Figure 3. We have shown that, for our processing and measurement protocols at least, surface morphology is not strongly correlated with $\phi\Sigma\mu$.[29] Another possibility is that the average structure of the perovskite is modified, and the electronic structure also changes. A simple way to quantify the structure of perovskites is using the Goldschmidt tolerance factor,[60] defined by Equation (1).

$$TF = \frac{r_A + r_X}{\sqrt{2(r_B + r_X)}} \tag{1}$$

Note that here we parameterize the tolerance factor with the symbol TF, rather than the more commonly used t, to avoid ambiguity with time in our TRMC measurements. Here r_A and r_B are the ionic radii of the A- and B-site cations, respectively, and r_X is the ionic radius of the anion. For perovskite structures, TF is bound between 0.8 and 1. In perovskite structures, a TF between 0.9 and 1 is known to result a cubic structure, and a TF between 0.8 and 0.9 is the orthorhombic phase. The tolerance factor can be indicative but is not a unique parameterization strategy, since two completely different structures, with different cation mixtures, may result in the same tolerance factor value. For instance, MA$_{0.4}$FA$_{0.6}$PbI$_3$ and FA$_{0.8}$Cs$_{0.2}$PbI$_3$ have the same tolerance factor. Moreover, MA and FA cations are organic compounds, rather than atoms, making it more challenging to define ionic diameter.

Here we have calculated the Goldschmidt tolerance factor calculated using the following radii $r_{MA} = 217$ pm, $r_{FA} = 253$ pm, $r_{Cs} = 181$ pm, $r_{Pb} = 133$ pm, and $r_I = 220$ pm. Since TF = 0.9 represents the boundary between cubic and orthorhombic phases, we could split our data into two groups: those with $0.8 < $ TF and ≤ 0.9 and those with $0.9 < $ TF ≤ 1. Instead, to consider all compounds in a single analysis, we have quantified our structures using the parameter $|TF - 0.9|$, that is, how far away from the cubic/orthorhombic boundary the structure is.

Figure 4a shows a scatterplot of $\phi\Sigma\mu$ plotted against the parameter $|TF - 0.9|$, and Figure 4b shows τ plotted against $|TF - 0.9|$. While there is significant scatter, there is a slight positive correlation between both $\phi\Sigma\mu$ and $|TF - 0.9|$, and τ and $|TF - 0.9|$, of 0.28 and 0.21, respectively. This suggests that structures with better defined cubic or orthorhombic structures could generally lead to better transport properties throughout the film. Although of course it is important not to read too much into relationships with this much variance, as there are clearly many other factors which play a role in transport besides this parameter. A more detailed analysis with a larger number of compositions would help determine statistical significance (if any).
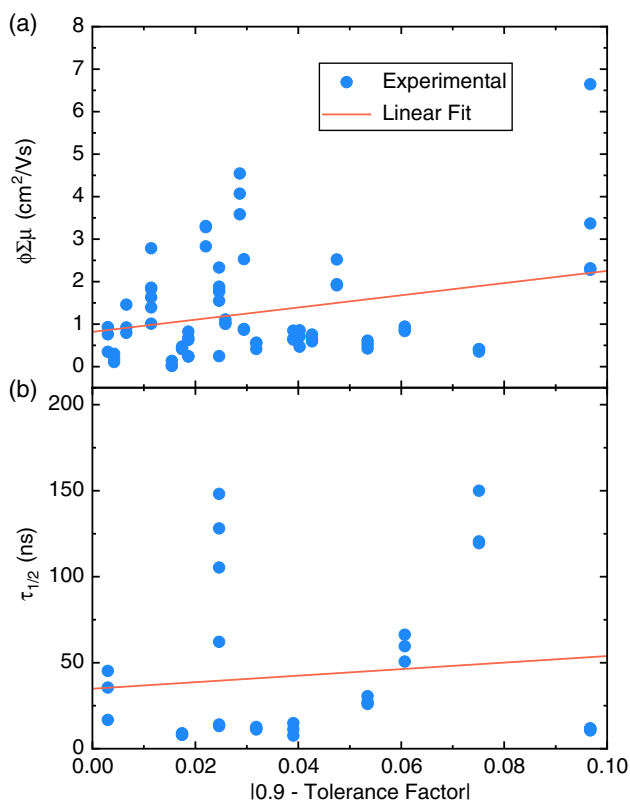
Figure 4. a) TRMC figure of merit $\phi\Sigma\mu$ of perovskite thin films evaluated using TRMC, as a function composition of the magnitude of the tolerance factor minus 0.9, $|TF - 0.9|$. b) Average carrier half life $\tau_{1/2}$, of same films plotted against $|TF - 0.9|$. Points are experimental values, and the lines are linear fits.

5. Conclusion

In this work, TRMC was applied to evaluate electronic properties of lead iodide perovskite thin films. The mobility-yield product and a proxy for lifetime were extracted and plotted for a range of cationic compositions, illustrating a strategy which can be built upon in the future. We found a general enhancement in mobility for the compounds with a single cation at the A-site: MAPbI$_3$, FAPbI$_3$, and CsPbI$_3$, but triple-cation compounds containing a small amount of cesium also exhibited high mobilities. By correlating these electronic properties with Goldschmidt tolerance factor, we found a small positive correlation with mobility when tolerance factor is between 0.9 and 1 but a negatively correlated behavior was observed for tolerance factor less than 0.9. This result suggests that as the structure becomes more stable, as quantified by from tolerance factor, the electronic performance generally improved.

6. Experimental Section

Methylammonium Lead Iodide (MAPbI$_3$) Thin Films: Lead iodide (PbI$_2$), methylammonium iodide (MAI), and dimethyl sulfoxide (DMSO) were mixed in a 1:1:1 molar ratio and then dissolved in dimethylformamide (DMF) at 3 mmol mL^{-1}. Chlorobenzene was used as antisolvent and then

the films were annealed at 100 °C for 10 min. MAI was purchased from GreatCell Solar and PbI$_2$ was purchased from Sigma Aldrich.

Formamidinium Lead Iodide (FAPbI$_3$) Thin Films: Lead iodide (PbI$_2$), formamidinium iodide (FAI), and dimethyl sulfoxide (DMSO) were mixed in a 1:1:1 molar ratio and then dissolved in dimethylformamide (DMF) at 3 mmol mL^{-1}. Chlorobenzene was used as antisolvent and then the films were annealed at 100 °C for 10 min. FAI and PbI$_2$ were purchased from Sigma Aldrich.

Cesium Lead Iodide (CsPbI$_3$) Thin Films: 0.8 M of CsI was dissolved in a mixture of DMF/DMSO at 4:1 volume ratio. CsI was purchased from Sigma Aldrich. The precursor solution was left for stirring for overnight. Films were spin cast onto clean quartz substrates. Two-step spin casting was applied: 1000 rpm for 10 s and then ramped up to 6000 rpm with acceleration of 4000 rpm for 1 min. Toluene was dripped 30 s before the spin-casting ends. The films stayed in air for 30 min before the annealing step. Films were annealed at 340 °C for 10 min.

MA$_x$FA$_{1-x}$PbI$_3$ Thin Films: Two master solutions MAPbI$_3$ and FAPbI$_3$ were prepared. They were then mixed with an appropriate ratio after being filtered individually.

MA$_x$Cs$_{1-x}$PbI$_3$ Thin Films: MAI and CsI salts were mixed in an appropriate ratio and then dissolved in a mixture of DMF/GBL at 97:3 volume ratio at 120 mg mL^{-1}. Toluene was used as antisolvent.

FA$_x$Cs$_{1-x}$PbI$_3$ Thin Films: FAI and CsI salts were mixed in an appropriate molar ratio and then dissolved in a mixture of DMF/DMSO at 3:1 volume ratio. Ether was used as antisolvent.

(MA$_{0.17}$FA$_{0.83}$)$_{1-x}$Cs$_x$Pb$_{I3}$ Thin Films: MA$_{0.17}$FA$_{0.83}$ solution was prepared from MAPbI$_3$ and FAPbI$_3$ master solutions. CsI was dissolved in DMSO at 390 mg mL^{-1}. CsI solution was then added to MA$_{0.17}$FA$_{0.83}$ mixture.

Time-Resolved Microwave Conductivity: The TRMC system used in this study was described in a previous report, and a brief description is provided here for completeness.[22] Microwaves were generated using a Sivers IMA VO4280X/00 voltage-controlled oscillator (VCO). The signal had an approximate power of 16dBm and a tunable frequency between 8 and 15 GHz. The VCO was powered with an NNS1512 TDK-Lambda constant 12 V power supply, and the output frequency was controlled by a Stahl Electronics BSA-Series voltage source. The sample was mounted inside the cavity at a maximum of the electric field component of the standing microwaves, using a 3D-printed PLA sample holder. Microwaves reflected from the cavity were then incident on a zero-bias Schottky diode detector (Fairview Microwave SMD0218). The detected voltage signal was amplified by a Femto HAS-X-1-40 high-speed amplifier (gain = ×100). The amplified detector voltage was measured as a function of time by a Textronix TDS 3032C digital oscilloscope. A Continuum Minilite II pulsed neodymium-doped yttrium aluminium garnet (Nd-YAG) laser was used to illuminate the sample. The laser pulse had a wavelength of 532 nm, FWHM≈5 ns, and a maximum fluence incident on the sample of ≈10^{15} photons cm^{-2} pulse^{-1}. An external trigger link was used to trigger the oscilloscope before the laser fires. The photoconductance and TRMC figure of merit $\phi\Sigma\mu$ were evaluated from changes in the detector voltage using standard analysis.[20]

UV–Vis Spectroscopy: UV–visible absorption spectra were obtained using a Shimadzu UV-Visible Spectrometer UV-2600 ranging from 200 to 1000 nm for all samples.

Statistical Analysis: Preprocessing of Data: Noise was subtracted from raw voltage versus time data by running a measurement with the beam blocked. No other filtering or preprocessing of transient data took place. No data points were removed.

Statistical Analysis: Data Presentation: Data points used in $\phi\Sigma\mu$ versus fluence and $\tau_{1/2}$ versus fluence plots (Figure 2) were means, and error bars were standard deviations. Points in Figure 3 were mean values of $\phi\Sigma\mu$ and $\tau_{1/2}$, and color gradients were linear interpolations between points, carried out with OriginLab Origin. Points shown in Figure 4 were individual data points (not mean values).

Statistical Analysis: Sample Size: Three samples were used for each mean and standard deviation of $\phi\Sigma\mu$ and $\tau_{1/2}$ plotted in Figure 2. 3 samples were used for each mean $\phi\Sigma\mu$ and $\tau_{1/2}$ values plotted in Figure 3.

Conflict of Interest

The authors declare no conflict of interest.

Data Availability Statement

The data that support the findings of this study are available from the corresponding author upon reasonable request.

Keywords

[1] A. Kojima, K. Teshima, Y. Shirai, T. Miyasaka, *J. Am. Chem. Soc.* **2009**, *131*, 6050.

[2] A. K. Jena, A. Kulkarni, T. Miyasaka, *Chem. Rev.* **2019**, *119*, 3036.

[3] C. Case, N. Beaumont, D. Kirk, *ACS Energy Lett.* **2019**, *4*, 2760.

[4] M. A. Green, E. D. Dunlop, J. Hohl-Ebinger, M. Yoshita, N. Kopidakis, X. Hao, *Progr. Photovolt. Res. Appl.* **2021**, *29*, 657.

[5] J. Y. Kim, J.-W. Lee, H. S. Jung, H. Shin, N.-G. Park, *Chem. Rev.* **2020**, *120*, 7867.

[6] M. M. Lee, J. Teuscher, T. Miyasaka, T. N. Murakami, H. J. Snaith, *Science* **2012**, *338*, 643.

[7] G. E. Eperon, S. D. Stranks, C. Menelaou, M. B. Johnston, L. M. Herz, H. J. Snaith, *Energy Environ. Sci.* **2014**, *7*, 982.

[8] M. Saliba, T. Matsui, J.-Y. Seo, K. Domanski, J.-P. Correa-Baena, M. K. Nazeeruddin, S. M. Zakeeruddin, W. Tress, A. Abate, A. Hagfeldt, M. Grätzel, *Energy Environ. Sci.* **2016**, *9*, 1989.

[9] M. Stolterfoht, C. M. Wolff, J. A. Márquez, S. Zhang, C. J. Hages, D. Rothhardt, S. Albrecht, P. L. Burn, P. Meredith, T. Unold, D. Neher, *Nat. Energy* **2018**, *3*, 847.

[10] D. P. McMeekin, G. Sadoughi, W. Rehman, G. E. Eperon, M. Saliba, M. T. Hörantner, A. Haghighirad, N. Sakai, L. Korte, B. Rech, M. B. Johnston, L. M. Herz, H. J. Snaith, *Science* **2016**, *351*, 151.

[11] Y.-H. Lin, N. Sakai, P. Da, J. Wu, H. C. Sansom, A. J. Ramadan, S. Mahesh, J. Liu, R. D. J. Oliver, J. Lim, L. Aspitarte, K. Sharma, P. K. Madhu, A. B. Morales-Vilches, P. K. Nayak, S. Bai, F. Gao, C. R. M. Grovenor, M. B. Johnston, J. G. Labram, J. R. Durrant, J. M. Ball, B. Wenger, B. Stannowski, H. J. Snaith, *Science* **2020**, *369*, 96.

[12] P. Roy, N. Kumar Sinha, S. Tiwari, A. Khare, *Sol. Energy* **2020**, *198*, 665.

[13] F. Brivio, A. B. Walker, A. Walsh, *APL Mater.* **2013**, *1*, 042111.

[14] E. L. Unger, L. Kegelmann, K. Suchan, D. Sörell, L. Korte, S. Albrecht, *J. Mater. Chem. A* **2017**, *5*, 11401.

[15] F. Xu, T. Zhang, G. Li, Y. Zhao, *J. Mater. Chem. A* **2017**, *5*, 11450.

[16] Z. Li, M. Yang, J.-S. Park, S.-H. Wei, J. J. Berry, K. Zhu, *Chem. Mater.* **2016**, *28*, 284.

[17] C. Yi, J. Luo, S. Meloni, A. Boziki, N. Ashari-Astani, C. Grätzel, S. M. Zakeeruddin, U. Röthlisberger, M. Grätzel, *Energy Environ. Sci.* **2016**, *9*, 656.

[18] C. C. Boyd, R. Cheacharoen, T. Leijtens, M. D. McGehee, *Chem. Rev.* **2019**, *119*, 3418.

[19] D. Guo, Z. Andaji Garmaroudi, M. Abdi-Jalebi, S. D. Stranks, T. J. Savenije, *ACS Energy Lett.* **2019**, 2360.

[20] T. J. Savenije, A. J. Ferguson, N. Kopidakis, G. Rumbles, *J. Phys. Chem. C* **2013**, *117*, 24085.

[21] H. Hempel, T. J. Savenije, M. Stolterfoht, J. Neu, M. Failla, V. C. Paingad, P. Kužel, E. J. Heilweil, J. A. Spies, M. Schleuning, J. Zhao, D. Friedrich, K. Schwarzburg, L. D. A. Siebbeles, P. Dörflinger, V. Dyakonov, R. Katoh, M. J. Hong, J. G. Labram, M. Monti, E. Butler-Caddle, J. Lloyd-Hughes, M. M. Taheri, J. B. Baxter, T. J. Magnanelli, S. Luo, J. M. Cardon, S. Ardo, T. Unold, *Adv. Energy Mater.* **2022**, *12*, 2102776.

[22] M. J. Hong, R. Y. Johnson, J. G. Labram, *J. Phys. Chem. Lett.* **2020**, *11*, 4976.

[23] S. K. Pal, T. Kesti, M. Maiti, F. Zhang, O. Inganäs, S. Hellström, M. R. Andersson, F. Oswald, F. Langa, T. Österman, T. Pascher, A. Yartsev, V. Sundström, *J. Am. Chem. Soc.* **2010**, *132*, 12440.

[24] M. Hilczer, M. Tachiya, *J. Phys. Chem. C* **2010**, *114*, 6808.

[25] A. Miyata, A. Mitioglu, P. Plochocka, O. Portugall, J. T.-W. Wang, S. D. Stranks, H. J. Snaith, R. J. Nicholas, *Nat. Phys.* **2015**, *11*, 582.

[26] J. G. Labram, M. L. Chabinyc, *J. Appl. Phys.* **2017**, *122*, 065501.

[27] R. B. Dunbar, B. C. Duck, T. Moriarty, K. F. Anderson, N. W. Duffy, C. J. Fell, J. Kim, A. Ho-Baillie, D. Vak, T. Duong, Y. Wu, K. Weber, A. Pascoe, Y.-B. Cheng, Q. Lin, P. L. Burn, R. Bhattacharjee, H. Wang, G. J. Wilson, *J. Mater. Chem. A* **2017**, *5*, 22542.

[28] E. M. Tennyson, T. A. S. Doherty, S. D. Stranks, *Nat. Rev. Mater.* **2019**, *4*, 573.

[29] M. J. Hong, J. G. Labram, *Adv. Funct. Mater.* **2021**, *31*, 2101843.

[30] J. Nelson, in *The Physics Of Solar Cells*, Imperial College Press, London, UK **2003**.

[31] I. Levine, S. Gupta, T. M. Brenner, D. Azulay, O. Millo, G. Hodes, D. Cahen, I. Balberg, *J. Phys. Chem. Lett.* **2016**, *7*, 5219.

[32] L. M. Herz, *Ann. Rev. Phys. Chem.* **2016**, *67*, 65.

[33] J. G. Labram, N. R. Venkatesan, C. J. Takacs, H. A. Evans, E. E. Perry, F. Wudl, M. L. Chabinyc, *J. Mater. Chem. C* **2017**, *5*, 5930.

[34] H. Oga, A. Saeki, Y. Ogomi, S. Hayase, S. Seki, *J. Am. Chem. Soc.* **2014**, *136*, 13818.

[35] O. G. Reid, M. Yang, N. Kopidakis, K. Zhu, G. Rumbles, *ACS Energy Lett.* **2016**, *1*, 561.

[36] E. M. Hutter, G. E. Eperon, S. D. Stranks, T. J. Savenije, *J. Phys. Chem. Lett.* **2015**, *6*, 3082.

[37] R. L. Milot, G. E. Eperon, H. J. Snaith, M. B. Johnston, L. M. Herz, *Adv. Funct. Mater.* **2015**, *25*, 6218.

[38] K. Wojciechowski, S. D. Stranks, A. Abate, G. Sadoughi, A. Sadhanala, N. Kopidakis, G. Rumbles, C.-Z. Li, R. H. Friend, A. K.-Y. Jen, H. J. Snaith, *ACS Nano* **2014**, *8*, 12701.

[39] G. Niu, W. Li, J. Li, X. Liang, L. Wang, *RSC Adv.* **2017**, *7*, 17473.

[40] J.-W. Lee, D.-H. Kim, H.-S. Kim, S.-W. Seo, S. M. Cho, N.-G. Park, *Adv. Energy Mater.* **2015**, *5*, 1501310.

[41] J. Zhao, V. M. Caselli, M. Bus, B. Boshuizen, T. J. Savenije, *ACS Appl. Mater. Interfaces* **2021**, *13*, 16309.

[42] Q. Dong, Y. Fang, Y. Shao, P. Mulligan, J. Qiu, L. Cao, J. Huang, *Science* **2015**, *347*, 967.

[43] Y. Chen, H. T. Yi, X. Wu, R. Haroldson, Y. N. Gartstein, Y. I. Rodionov, K. S. Tikhonov, A. Zakhidov, X.-Y. Zhu, V. Podzorov, *Nat. Commun.* **2016**, *7*, ncomms12253.

[44] X. Y. Chin, D. Cortecchia, J. Yin, A. Bruno, C. Soci, *Nat. Commun.* **2015**, *6*, 7383.

[45] A.-F. Castro-Méndez, J. Hidalgo, J.-P. Correa-Baena, *Adv. Energy Mater.* **2019**, *9*, 1901489.

[46] J.-S. Park, A. Walsh, *Ann. Rev. Condens. Matter Phys.* **2021**, *12*, 95.

[47] G. W. P. Adhyaksa, S. Brittman, H. Āboliņš, A. Lof, X. Li, J. D. Keelor, Y. Luo, T. Duevski, R. M. A. Heeren, S. R. Ellis, D. P. Fenning, E. C. Garnett, *Adv. Mater.* **2018**, *30*, 1804792.

[48] J. S. Yun, A. Ho-Baillie, S. Huang, S. H. Woo, Y. Heo, J. Seidel, F. Huang, Y.-B. Cheng, M. A. Green, *J. Phys. Chem. Lett.* **2015**, *6*, 875.

[49] Z. Chu, M. Yang, P. Schulz, D. Wu, X. Ma, E. Seifert, L. Sun, X. Li, K. Zhu, K. Lai, *Nat. Commun.* **2017**, *8*, 1.

[50] W.-J. Yin, T. Shi, Y. Yan, *Appl. Phys. Lett.* **2014**, *104*, 063903.

[51] Y. Zhao, A. M. Nardes, K. Zhu, *J. Phys. Chem. Lett.* **2014**, *5*, 490.

[52] Y. Li, W. Yan, Y. Li, S. Wang, W. Wang, Z. Bian, L. Xiao, Q. Gong, *Sci. Rep.* **2015**, *5*, 14485.

[53] D. W. de Quilettes, S. M. Vorpahl, S. D. Stranks, H. Nagaoka, G. E. Eperon, M. E. Ziffer, H. J. Snaith, D. S. Ginger, *Science* **2015**, *348*, 683.

[54] B. S. Tosun, H. W. Hillhouse, *J. Phys. Chem. Lett.* **2015**, *6*, 2503.

[55] R. Long, J. Liu, O. V. Prezhdo, *J. Am. Chem. Soc.* **2016**, *138*, 3884.

[56] H. D. Kim, H. Ohkita, H. Benten, S. Ito, *Adv. Mater.* **2016**, *28*, 917.

[57] A. R. Pascoe, M. Yang, N. Kopidakis, K. Zhu, M. O. Reese, G. Rumbles, M. Fekete, N. W. Duffy, Y.-B. Cheng, *Nano Energy* **2016**, *22*, 439.

[58] J.-H. Im, H.-S. Kim, N.-G. Park, *APL Mater.* **2014**, *2*, 081510.

[59] X. Ren, Z. Yang, D. Yang, X. Zhang, D. Cui, Y. Liu, Q. Wei, H. Fan, S. (Frank) Liu, *Nanoscale* **2016**, *8*, 3816.

[60] W. Travis, E. N. K. Glover, H. Bronstein, D. O. Scanlon, R. G. Palgrave, *Chem. Sci.* **2016**, *7*, 4548.